ohio2/yjp-yjp/yjp-yjp/yjp99907/yjp5511d07z | xppws | 23:ver.3 | 6/28/08 | 12:23 | Msc: jp-2008-014194 | TEID: pjp00 | BATID: jp8c112

Orientational Ordering of Crystal Domains in Ionic Liquid Based Mixtures

Yusuke Imai,[†] Hiroshi Abe,*[,†] Takefumi Goto,[‡] Yukihiro Yoshimura,[‡] Shogo Kushiyama,[†] and Hitoshi Matsumoto[†]

Department of Materials Science and Engineering, and Department of Applied Chemistry, National Defense Academy, Yokosuka 239-8686, Japan

Received: February 18, 2008; Revised Manuscript Received: May 16, 2008

By in situ observations using simultaneous X-ray diffraction and the DSC (differential scanning calorimetry) method, the effect of water, methanol, ethanol, and benzene on the crystallization has been observed in an ionic liquid (IL)-rich phase. The IL is a hydrophilic ionic liquid, *N*,*N*-diethyl-*N*-methyl-*N*-2-methoxyethyl ammonium tetrafluoroborate, [DEME][BF_4]. At a small amount of the above additional molecules in the IL, the conventional preferred orientation on the Debye rings was seen by the X-ray diffraction. At 0.9 mol % H_2O, twinlike crystal domains develop extraordinary on the microdomains. By the "crystal-growth enhancement effect" at a slight amount of water, a composite domain structure, which consists of the large domain and the weakly orientated microdomains, is formed without internal strains. Above 2.9 mol % H_2O, the domain structure, however, disappears completely. It is remarkable that, in a thermal cycling experiment using pure [DEME][BF_4], the similar composite domain structure appeared. This is also caused by an uptake of a slight amount of water.

1. Introduction

Room-temperature ionic liquids (ILs) basically consist of a large organic cation and a smaller organic or inorganic anion that is molten. ILs attract much attention as environmentally friendly solvents.[1,2] In green chemistry, ILs are applied into clean solvents, catalysis,[3] photochemistry, and electrosynthesis.[4] Peculiar features of ILs are almost zero vapor pressure, high electrical conductivity, and a wide electrochemical window.[5]

Another important feature of ILs is that ILs easily absorb water molecules from the atmosphere.[5,6] Many studies on the water−IL mixtures have been reported so far as follows. Solubility of water in ILs was studied systematically in the water−IL binary systems.[6] It was found that the IL-rich phase is estimated to be a different phase with a pure IL one, although the water-rich phase is considered to be an almost pure water phase. By ATR (attenuated total reflection) and transmission IR spectroscopy, the dynamic property of dissolved water in ILs was investigated both in 1-butyl-3-methylimidazolium $[bmim]^+$- and 1-butyl-2,3,4,5-tetramethylimidazolium $[bm_4im]^+$-based salts.[7] Dissolved water molecules interact preferably with anions. Recently, rotational dynamics of water was examined by ^1H NMR spin−lattice relaxation time measurements.[8] Water rotates in hydrophilic [bmim][Cl] twice as slowly as in hydrophobic [bmim][PF_6]. Moreover, vibration modes of [bmim][BF_4]−water mixtures were observed by ATR infrared absorption and Raman spectroscopy,[9] reporting that [bmim][BF_4] breaks an intrinsic hydrogen-bonding network of water molecules drastically. In molecular dynamics simulations,[10] water behavior in [dmim]Cl and [dmim][PF_6] was simulated. The local structure and the dynamics of the mixtures were analyzed over the wide range of water concentration. At the IL-rich phase, water molecules tend to be isolated from each other in the mixtures, although a continuous water network appears at the water-rich phase. Other molecular dynamics simulations showed the significant nanostructual organization in 1-octyl-3-methylimidazolium nitrate IL−water mixtures.[11] Nonpolar and polar phase separation occurs on the nanoscale. Each polar region is linked by a water molecule at the IL-rich phase. Recently, a phase transition on the surface of the water-rich phase is reported.[12] The surface transition is studied in the water-rich phase of water−IL mixtures, [bmim][BF_4] and 1-butyl-2, 3-dimethylimidazolium [bdmim][BF_4]. The discontinuous surface thermal coefficient exhibits a transition such as an aggregation.

Recently, *N*,*N*-diethyl-*N*-methyl-*N*-2-methoxyethyl ammonium tetrafluoroborate, [DEME][BF_4], as a different kind of IL, is synthesized for electrochemical capacitors, which has a quite wide potential window.[13] Fundamental physical properties of [DEME][BF_4] were examined. Furthermore, we have reported anomalous phase transition behavior in [DEME][BF_4]−water mixtures by simultaneous X-ray and differential scanning calorimetry (DSC) measurements.[14] A complicated phase diagram in the range from 0.0 to 12.0 mol % H_2O was obtained both on cooling and heating processes. For instance, pure amorphous phase appears only at ≈6 mol % H_2O. In addition, "two different dynamic components" in the Raman spectrum are observed in the amorphous phase: one is liquid-like, and the other is crystal-like. On the other hand, upon heating, a cold crystallization[15] appears above 4 mol % H_2O.

Thus, in this study, we focus on crystal domain formations in several [DEME][BF_4]-based mixtures; additional molecules are water, methanol, ethanol, and benzene. The developments of crystal domains are observed by simultaneous X-ray and DSC measurements. By comparing with mixtures of organic solvents, we clarify the anomalous "water effect" on the [DEME][BF_4]−water mixtures and the "thermal cycling effect" for the pure [DEME][BF_4]. In the former effect, the composite domain structure, which consists of large twinlike crystal domains and conventional microdomains, appears at a specific region of water concentration. In the latter effect, the composite domain structure

* Corresponding author.
[†] Department of Materials Science and Engineering.
[‡] Department of Applied Chemistry.

10.1021/jp8014194 CCC: $40.75

ohio2/yjp-yjp/yjp-yjp/yjp99907/yjp5511d07z | xppws | 23:ver.3 | 6/28/08 | 12:24 | Msc: jp-2008-014194 | TEID: pjp00 | BATID: jp8c112

appears at the fifth thermal cycle. This is caused by a slight accumulation of uptake water at each cycling. Importantly in both effects, the composite domain structure is formed by the "crystal-growth enhancement effect" at a slight amount of water.

2. Experimental Section

2.1. Materials. In this study, we used the ionic liquid *N*,*N*-diethyl-*N*-methyl-*N*-2-methoxyethyl ammonium tetrafluoroborate (Kanto Chemical Co.) [DEME][BF_4]. [DEME][BF_4] is hydrophilic, and the water concentration is estimated to be 126 ppm as received. Generally, the ILs are contaminated easily by vacuum drying to reduce H_2O; thus, we used the sample without further purification. In this study, we carried out two kinds of experiments: one is the "thermal cycling effect" in the [DEME][BF_4], and the other is "water effect" in the [DEME]-[BF_4]−water mixtures as a function of water concentration. The former experiments were done with continuously repeated five cycle runs, but without changing the sample. For water mixtures in the [DEME][BF_4]-rich phase, we used distilled water (Wako Pure Chemical Co.) Water concentrations, x, investigated in this study were 0.0, 0.6, 0.9, 2.9, and 4.4 mol % H_2O. Methanol (x = 0.8 and 7.3 mol %), ethanol (x = 1.2 and 6.7 mol %), and benzene (1.1 and 6.1 mol %) (Wako Pure Chemical Co.) mixtures of [DEME][BF_4] were also measured in order to compare with the water mixtures.

2.2. Instrumentation. In situ simultaneous observations were performed using X-ray diffraction and DSC. The DSC is attached on a vertical goniometer with 3 kW X-ray generator (RINT-Ultima III, Rigaku Co., Japan). For in situ observations of liquid, a sample stage is fixed horizontally. A sealed X-ray tube and a scintillation counter are moving simultaneously. A parallel beam is obtained by a parabolic multilayer mirror. A long soller slit is placed in front of the scintillation counter. Cu Kα radiation ($\lambda = 0.1542$ nm) was selected for the simultaneous measurements. The X-ray source was generated using an applied voltage of 40 kV and a filament current of 50 mA. The reciprocal lattice unit is $q = 4\pi(\sin\theta)/\lambda$ (nm^{-1}), where q is the scattering wave vector. In this optics, resolution function is estimated by measuring a standard Si polycrystal. DSC windows for X-ray are metal-coated Mylar films. Observed temperatures were corrected by standard In measurements. During simultaneous measurements, dry N_2 gas was flowing at 20 cc/min in order to reduce moisture.

2.3. Method. In this study, two kinds of scan modes ($\theta-2\theta$ and θ scans) were carried out. For conventional diffraction patterns, the $\theta-2\theta$ scan was used. The $\theta-2\theta$ scan mode is the radial scan in reciprocal space. Peak shifts and widths along the radial scan contain information of lattice distortions, while the direction of the θ scan is transverse in reciprocal space. The θ scan represents the preferred orientation on the Debye ring of a polycrystalline and mosaicity of a single crystal. Peak widths along the transverse direction contain information of crystal domain formation.

3. Results

3.1. Phase Transition of Pure [DEME][BF_4] at the First Thermal Cycle. Figure 1a shows DSC thermograms of pure [DEME][BF_4] at the first thermal cycle, where the cooling and heating rate was 8.5 and 3.0 °C/min, respectively. Thermograms on heating exhibit two melting endotherms. As an advantage for in situ simultaneous observations of X-ray diffraction and DSC, we can determine transition temperatures, denoted as T_{m1} and T_{m2}, more precisely as shown in Figure 1, parts b and c. It was found in a previous study[14] that crystal structures below T_c are orthorhombic space group $C222_1$ with a = 1.8997, b = 1.8957, c = 1.1987 (nm) and monoclinic space group $P2_1$ with a = 0.9285, b = 1.3476, c = 0.7778 (nm), β = 105.9 °. Closed squares and open circles in Figure 1c reveal orthorhombic and monoclinic, respectively.

Some part of the diffraction patterns in Figure 1c is enlarged as shown in Figure 2a. In the detailed diffraction patterns upon heating, we find that peak separations along the radial direction become larger with increasing temperature. These peak separations are indicated by thick arrows in the figure. In order to clarify the temperature dependence of the peak separations, peak positions both on cooling and heating are calculated by peak profile fitting using a pseudo-Voigt function. Figure 2b shows the largest peak separation of Bragg reflections. There is a tendency that weak Bragg reflections shift largely to smaller scattered angles on the thermal cycling, whereas sharp and strong ones shift a little.

As an another approach to phase transitions, strain analysis in X-ray diffraction is quite important. Figure 3 reveals the fwhm (full widths at half-maximum) of the Bragg peak along the radial direction at the first thermal cycle, cycle 1, as a function of q. For a comparison, the resolution function, which is determined by measuring a standard Si polycrystal, is displayed in Figure 3. Considering no peak broadening along the radial direction, it is clear that crystal microdomains are formed without internal strains.

3.2. Preferred Orientation of Crystal Domains at Each Thermal Cycling. Drastic changes of rocking curves (θ scan) in X-ray diffraction are observed at each thermal cycling using pure [DEME][BF_4]. No difference of diffraction patterns along the radial direction is, however, seen through the all thermal cyclings. Figure 4 shows rocking curves along the transverse direction. The thermal cycling dependence of the rocking curves is measured at fixed 2θ (=17.4°), where the temperature is −70 °C. The fixed 2θ position of the Bragg reflection is indicated by the thick arrow in Figure 1b. Obviously, preferred orientation on the Debye ring becomes remarkable with increasing the number of thermal cycles. At cycles 3 and 4, the common preferred orientation of the Debye ring is observed. In addition to the common preferred orientation, sharp and strong Bragg reflections appear at cycle 5. Mosaicity of crystal domains derived from the strong and sharp peaks is estimated to be 0.1°. Moreover, strong Bragg reflections in the [DEME][BF_4] have a specific orientational relation of twin-crystal structure, such as is observable in shape memory alloys.[16,17] A twinlike structure is represented by a pair of peak splittings. In general, a complicated domain structure such as above might cause intrinsic strains. Nevertheless, no peak broadening at cycle 5 is observed along the radial direction as shown in Figure 3.

If we see the rocking curves as a function of temperature, the "thermal cycling effect" is expected to be clearer. Figure 5a shows the temperature dependence of the rocking curves at cycle 3, where the heating rate was 3 °C/min and the fixed 2θ value is 17.4°. The peak shifts at cycle 5 are indicated by arrows (Figure 5b). There is a tendency that weak Bragg peaks shift their positions continuously and sharp ones remains at fixed θ value ($T < T_{m1}$). On further heating ($T_{m1} < T < T_{m2}$), peak positions of weak Bragg reflections change randomly, whereas sharp ones shift continuously.

3.3. Preferred Orientation of Crystal Domains in [DEME][BF_4]−Water Mixtures. Since [DEME][BF_4] is hydrophilic, it is considered that the "thermal cycling effect" is derived from additional water absorbed from the environment. But unfortunately, the amount of absorbed water in pure

ohio2/yjp-yjp/yjp-yjp/yjp99907/yjp5511d07z | xppws | 23:ver.3 | 6/28/08 | 12:24 | Msc: jp-2008-014194 | TEID: pjp00 | BATID: jp8c112

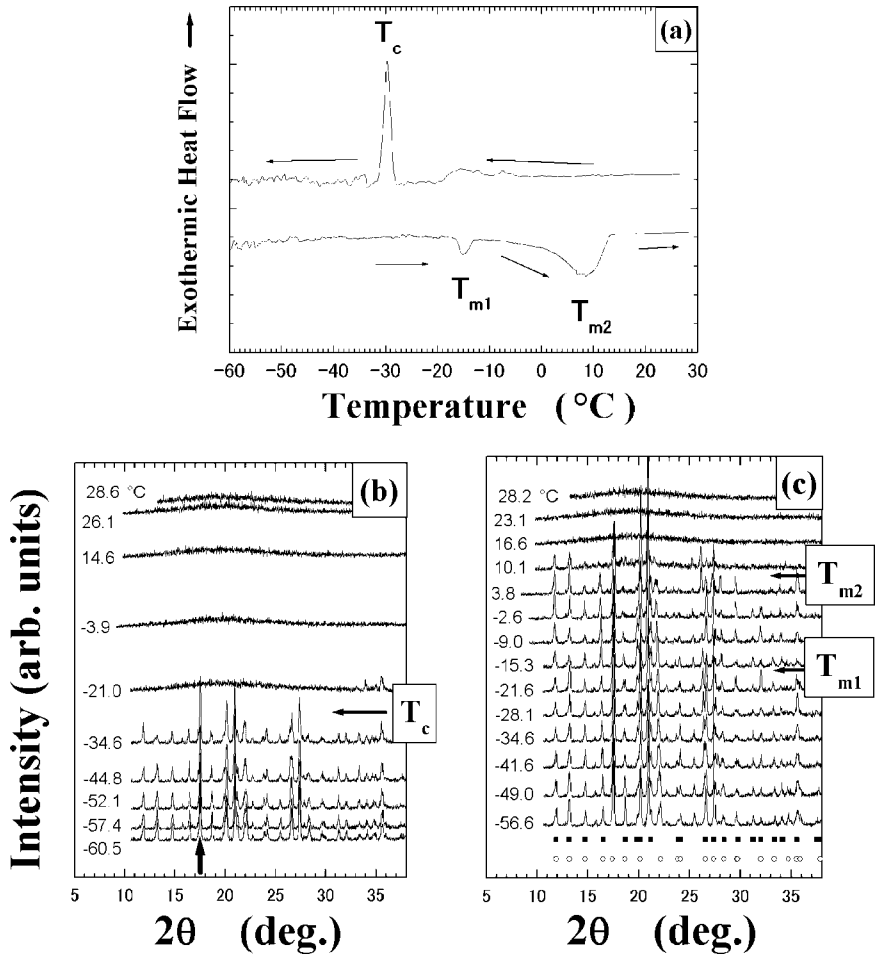

Figure 1. Simultaneous X-ray diffraction and DSC measurements at the first thermal cycle using pure [DEME][BF_4]. (a) Thermographs on cooling and heating by DSC; X-ray diffraction patterns along the radial direction on (b) cooling and (c) heating. Closed squares and open circles correspond to calculated 2θ values of orthorhombic and monoclinic, respectively (see ref 7). The cooling rate was 8.5 °C/min, and the heating one was 3 °C/min. T_c, T_{m1}, and T_{m2} reveal crystallization temperature, the first melting point, and the second one, respectively.

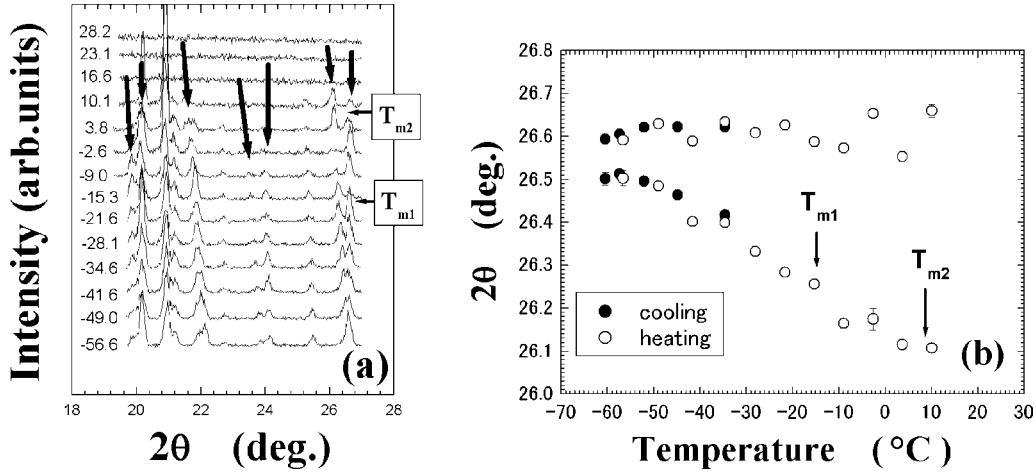

Figure 2. (a) Enlarged X-ray diffraction pattern along the radial direction of Figure 1c. (b) Temperature dependence of the peak position of Bragg reflections. Peak separations of the Bragg refection are observed both on cooling and heating.

[DEME][BF_4] in the thermal cycling run is not estimated precisely. Therefore, we have investigated [DEME][BF_4]−water mixtures as a function of water concentration x ($0.0\% < x < 4.4\%$, x: mole fraction of water) by simultaneous X-ray diffraction and DSC measurements. Interestingly, X-ray diffraction patterns do not depend on the water concentration. Furthermore, no peak broadening of Bragg reflections along the radial direction is observed at the studied water concentration region. In contrast, rocking curves in the [DEME][BF_4]−water mixtures obtained at fixed 2θ value (17.4°) vary sensitively even in a slight amount of water (Figure 6). Below 0.6 mol % H_2O, the common preferred orientation on the Debye ring is observed. At 0.9%, highly preferred orientation appears extraordinary on the Debye ring. It is to be noted that the rocking curve is similar to that at cycle 5 using pure [DEME][BF_4] (Figure 4). Above 2.9%, the preferred orientation disappears completely. It is clear

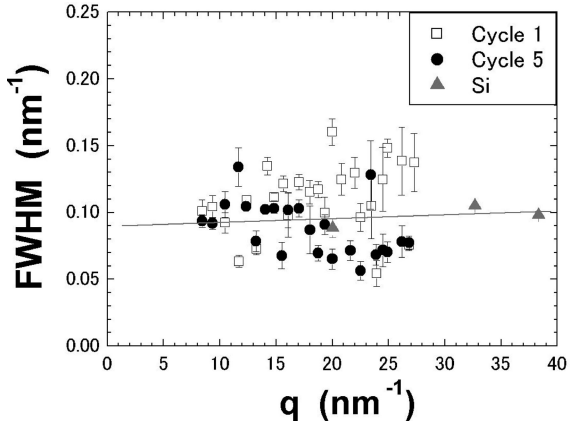

Figure 3. The q dependence of the full width at half-maximum (fwhm) of the Bragg reflection along the radial direction at the first and fifth thermal cycles using pure [DEME][BF_4]. As a resolution function in the beam optics, Bragg reflections of a standard Si polycrystal are measured.

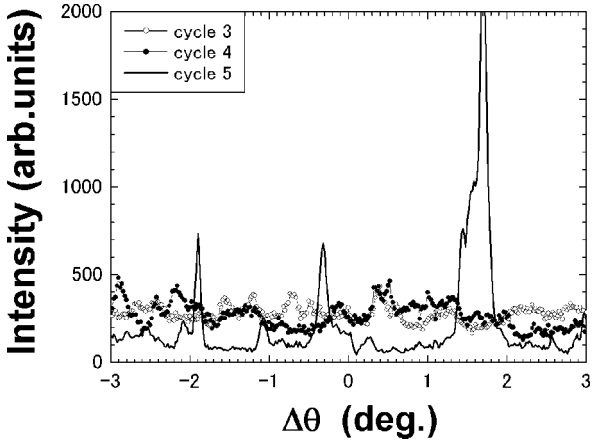

Figure 4. Rocking curves (transverse direction) at the third, fourth, and fifth thermal cycles at −70 °C using pure [DEME][BF_4]. At the fifth thermal cycle, preferred orientation of crystal domains is remarkably observed.

that the randomly orientated microdomains are formed by a small increase of water content.

3.4. Preferred Orientation of Crystal Domains in Other Mixtures of Organic Solvents. Crystal structure of other mixtures except water, that is, [DEME][BF_4]−methanol, [DEME][BF_4]−ethanol, and [DEME][BF_4]−benzene, are found to be almost the same as that of pure [DEME][BF_4]. Also, no strain appears in the mixtures as indicated by fwhm of Bragg reflections along the radial scan. Figure 7 shows rocking curves in [DEME][BF_4]−methanol, [DEME][BF_4]−ethanol, and [DEME][BF_4]−benzene. In the mixtures other than ethanol, apparent preferred orientations on the Debye rings are observed at both around 1 and 6 mol %, respectively. However, only the mixture of 1.2 mol % C_2H_5OH has no preferred orientation. Thus, compared with the result of [DEME][BF_4]−water mixtures, the opposite tendency on the concentration effect for the preferred orientation appears in the [DEME][BF_4]−ethanol mixture.

4. Discussion

In former studies, two influences of water absorbed into ILs were discussed. One is absorption of water from the atmospheric air as a function of time.[5,7,18] The other is the solubility of water as a function of temperature.[6] As a hydrophilic IL system such as $[P(C_6)_3C_{14}]^+$, $[Br]^-$, $[Cl]^-$, $[BF_4]^-$ contains a little water,[18] it is estimated that each sample contains approximately 0.1 wt % H_2O. It is also reported that ILs are contaminated easily by vacuum drying to reduce H_2O. In the present study, we have examined the water influence on the IL by viewpoints from "thermal cycling effect" and "water addition effect".

At first, we mention the "water addition effect" in a binary system. We have observed three types of crystal domain structures at a specific region of water concentration by the simultaneous X-ray and DSC: type I is conventional microdomains (x < 0.6 mol % H_2O), which have weak orientational relationships. Type II is a "composite domain structure" (x = 0.9 mol %), which consists of conventional microdomains and large twin-related domains. Type III is randomly orientated microdomains (x > 2.9 mol %). Quite fine domains or particles have little preferred orientation of the ideal Debye ring, although the fine size provides the broad peak along the radial direction. Since type III has neither a preferred orientation nor peak broadening along the radial direction, the domain structure of type III is extremely curious. Furthermore, we emphasize that three types of domain structures are influenced extensively by only a slight amount of water. It is interesting to point out that the crystal structure of the [DEME][BF_4]−water mixtures does not change at water concentrations of 0.0 < x < 4.4 mol %. Therefore, as for the water-induced growth enhancement of the crystal domain, a slight amount of water contributes only to the domain formations, not to structural changes of the crystal. The anomalous domain growth induced by water is emphasized by comparing with other mixtures. That is, no randomly orientated microdomains appear on [DEME][BF_4]−methanol and [DEME][BF_4]−benzene mixtures at around 1 and 6 mol %. General domain growth is not suppressed by addition of methanol or benzene. On the other hand, almost no preferred orientation on the Debye ring is observed at 1.2 mol % C_2H_5OH. It is predicted that fine domain formation of 1.2 mol % C_2H_5OH may connected with somewhat peculiar local interaction between ethanol and [DEME] molecules on a nanoscale.

Here we have to mention about the role of water in the crystallization processes to describe the curious behavior of domain formations. In general, a large twin-related domain is formed not by local defects but by macroscopic elasticity. Therefore, it is difficult to consider that quite a small difference in the H_2O content can control the crystal domain formation over the mesoscopic region. Recently, the key to resolve the problem is proposed. Annapureddy et al.[19] found that water screens the direct Coulombic interactions between cations and anions and that it facilitates rotational and translational motion in the presence of small amounts of water.

Alternatively, the information from the effect of other solvents except water on the crystallization like done in this study may help us to understand the role of water. In this relation, it is interesting to quote that Miki et al.[20] have studied a ternary system, 1-propanol-1-butyl-3-methylimidazolium chloride−H_2O, in order to use the behavior of 1-propanol as a probe for the effect of the IL on the molecular organization of H_2O in the H_2O-rich region. They speculated that the bulk H_2O is influenced by the third molecule as many H_2O molecules are attracted to the delocalized positive charge of the cation. However, we note that the properties might depend on ILs, i.e., not all ILs show the same behavior, and also the solution structure depends on the composition range of the mixtures, e.g., water-rich and water-poor regions.[21] These kinds of experiments with changing solvent properties vastly, e.g., the dielectric constant of the solvent, are necessary, though this is beyond the present study.

ohio2/yjp-yjp/yjp-yjp/yjp99907/yjp5511d07z | xppws | 23:ver.3 | 6/28/08 | 12:24 | Msc: jp-2008-014194 | TEID: pjp00 | BATID: jp8c112

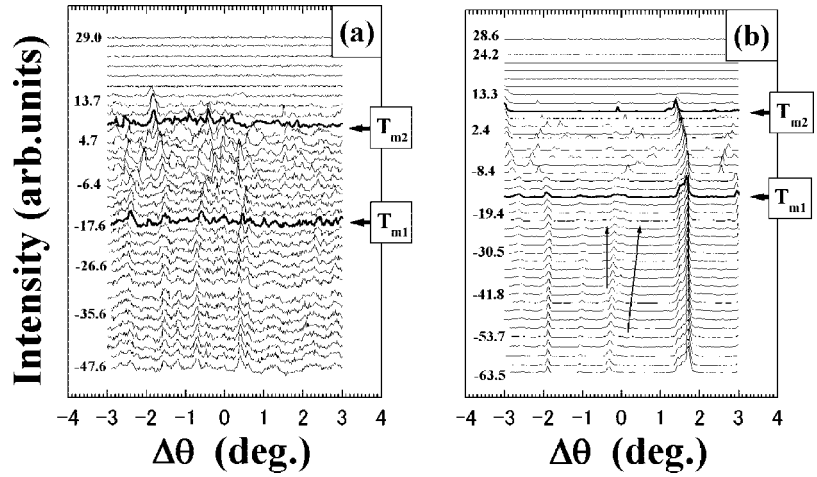

Figure 5. Rocking curves as a function of temperature at (a) the third and (b) the fifth thermal cycles (pure [DEME][BF_4]). The heating rate was 3 °C/min. The rocking curves at T_{m1} and T_{m2} are shown as thick curves.

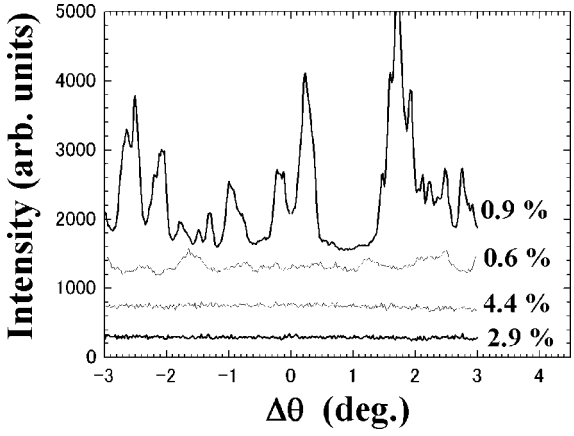

Figure 6. Concentration dependence of water for the rocking curve at −70 °C. Extensive preferred orientation occurs at a specific region of water concentration in [DEME][BF_4]−water mixtures.

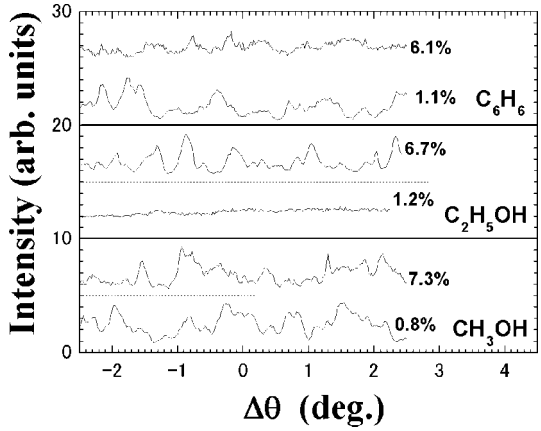

Figure 7. Rocking curves of [DEME][BF_4]−methanol, [DEME]-[BF_4]−ethanol, and [DEME][BF_4]−benzene mixtures.

Second, we consider the "thermal cycling effect" in pure [DEME][BF_4]. It is certain that the "thermal cycling effect" is caused by the water contamination at each thermal cycling in pure [DEME][BF_4]. A drastic change in the rocking curve is observed at the fifth thermal cycle (cycle 5). Quite sharp and strong Bragg reflections appear on the broad and weak Debye ring. The domain structure at cycle 5 is almost the same as the type II domain structure described above. If we assume that water contamination at each cycling is estimated to be 0.1−0.2 mol % H_2O, domain structures at cycles 4 and 5 are explained by formations of type I (x = 0.6 mol %) and type II (x = 0.9 mol %) structures, respectively. Consequently, the composite domain structure like one in shape memory alloys[16,17] is formed in water-contained [DEME][BF_4]. Quite a slight amount of water plays an important role for the domain growth or cooperative orientational ordering of the microdomains.

Dynamics in the composite domain structure is important to evaluate interactions between domains. In a crystal phase (C phase) at $T < T_{m1}$, continuous peak shifts of weak Bragg reflections and no shifts of sharp and strong ones are observed on heating. In the C phase on heating, weakly orientational ordered microdomains are thermally activated followed by a gradual rotation of the domain. In a crystal + liquid phase ((C + L) phase) at $T_{m1} < T < T_{m2}$, random peak shifts of weak Bragg reflections and continuous peak shifts of sharp and strong ones are observed. It is supposed that, in the (C + L) phase on heating, the microdomains rotate randomly because of the random motion of liquid molecules. At the same stage ($T_{m1} < T < T_{m2}$), large twin-related domains rotate continuously inside randomly rotated microdomains with increasing temperature.

5. Remarks

In this study, we have shown an importance of the "water-induced growth enhancement of crystal domains" at a slight amount of water in the IL-rich phase. The main results are summarized as follows: (i) three types of domain structure appear at a specific region of water concentration. (ii) The small amount of water absorbed into the IL increases at each thermal cycling in spite of the dry N_2 gas flowing. (iii) No internal strains are generated, and the crystal structure does not change even in the composite domain structure. The water-assist domain formations are a fascinating property in the [DEME][BF_4]-rich phase. Domain formations in the present system are classified into three types; (I) weakly orientated microdomains (x < 0.7%), (II) composite domain structure of the weakly orientated microdomains and large twin-related domains (x = 0.9%), and (III) ideal randomly orientated microdomains (x > 2.0%). Since the composite domain structure appears only at the limited water concentration, it is evident that a well-organized domain structure without internal strains is maintained by a slight amount of water. We confirm that a suitable amount of water molecules contributes greatly to the growth process and coarsening. But if we put "excess" water molecules to the system, the growth of microdomains is in turn suppressed. On

ohio2/yjp-yjp/yjp-yjp/yjp99907/yjp5511d07z | xppws | 23:ver.3 | 6/28/08 | 12:24 | Msc: jp-2008-014194 | TEID: pjp00 | BATID: jp8c112

the contrary, no randomly orientated microdomains appear as to the mixtures with organic solvents, though type III domain formation is observed at 1.2 mol % C_2H_5OH. As the anomalous behavior of water molecules in the IL-rich phase remains unclear, more continuous study is needed. It would also help for clarifying an essential feature of water molecules[22] in a polymer system.

Acknowledgment. We appreciate Ms. M. Sasaki of Rigaku Co. and Mr. A. Kishi of Rigaku Co. for experimental support and helpful discussions

References and Notes

(1) Welton, T. *Chem. Rev.* **1999**, *99*, 2071.
(2) Earle, M. J.; Seddon, K. R. *Pure Appl. Chem.* **2000**, *72*, 1391.
(3) Sheldon, R. *Chem. Commun.* **2001**, 2399.
(4) Hussey, C. L. *Electrochemistry* **1996**, *76*, 527.
(5) Seddon, K. R.; Stark, A.; Torres, M.-J. *Pure Appl. Chem.* **2000**, *72*, 2275.
(6) Freire, M. G.; Neves, C. M. S. S.; Carvalho, P. J.; Gardas, R. L.; Fernandes, A. M.; Marrucho, I. M.; Santos, L. M. N. B. F.; Coutinho, J. A. P. *J. Phys. Chem. B* **2007**, *111*, 13082.
(7) Cammarata, L.; Kazarian, S. G.; Salter, P. A.; Welton, T. *Phys. Chem. Chem. Phys.* **2001**, *3*, 5192.
(8) Yasaka, Y.; Wakai, C.; Matubayashi, N.; Nakahara, M. *J. Chem. Phys.* **2007**, *127*, 104506.
(9) Jeon, Y.; Sung, J.; Kim, D.; Seo, C.; Cheong, H.; Ouchi, Y.; Ozawa, R.; Hamaguchi, H. *J. Phys. Chem. B* **2008**, *112*, 923.
(10) Hanke, C. G.; Lynden-Bell, R. M. *J. Phys. Chem. B* **2003**, *107*, 10873.
(11) Jiang, W.; Wang, Y.; Voth, G. A. *J. Phys. Chem. B* **2007**, *111*, 4812.
(12) Malham, I. B.; Letellier, P.; Turmine, M. *J. Phys. Chem. B* **2006**, *110*, 14212.
(13) Sato, T.; Masuda, G.; Takagi, K. *Electrochim. Acta* **2004**, *49*, 3603.
(14) Abe, H.; Imai, Y.; Goto, T.; Yoshimura, Y. *Chem. Phys.*, submitted for publication.
(15) Mukai, T.; Yoshio, M.; Kato, T.; Yoshizawa, M.; Ohno, H. *Chem. Commun.* **2005**, 1333.
(16) Abe, H.; Ishibashi, M.; Ohshima, K.; Suzuki, T.; Wuttig, M.; Kakurai, K. *Phys. Rev. B* **1994**, *50*, 9020.
(17) Condo, A. M.; Lovey, F. C.; Torra, V. *Philos. Mag.* **2003**, *83*, 1479.
(18) Ito, N.; Arzhantsev, S.; Heitz, M.; Maroncelli, M. *J. Phys. Chem. B* **2004**, *108*, 5771.
(19) Annapureddy, H. V. R.; Hu, Z.; Xia, J.; Margulis, C. J. *J. Phys. Chem. B* **2008**, *112*, 1770.
(20) Miki, K.; Westh, P.; Nishikawa, K.; Koga, Y. *J. Phys. Chem. B* **2005**, *109*, 9014.
(21) Katayanagi, H.; Nishikawa, K.; Shimozaki, H.; Miki, K.; Westh, P.; Koga, Y. *J. Phys. Chem. B* **2004**, *108*, 19451.
(22) Scatena, L. F.; Brown, M. G.; Richmond, G. L. *Science* **2001**, *292*, 908.

JP8014194